ACS APPLIED MATERIALS & INTERFACES

Research Article

www.acsami.org

Photochemistry-Based Method for the Fabrication of SnO_2 Monolayer Ordered Porous Films with Size-Tunable Surface Pores for Direct Application in Resistive-Type Gas Sensor

Shipu Xu,[†] Fengqiang Sun,*[,†,‡,§] Fenglong Gu,[†,‡] Yanbing Zuo,[†] Lihe Zhang,[†] Caifeng Fan,[†] Shumin Yang,[†] and Weishan Li[†]

[†]School of Chemistry and Environment, South China Normal University, Guangzhou 510006, P. R. China

[‡]Key Laboratory of Theoretical Chemistry of Environment, Ministry of Education, South China Normal University, Guangzhou 510631, P. R. China

[§]Exhibition Base of Production, Study & Research on New Polymer Materials and Postgraduate Students' Innovation Training of Guangdong Higher Education Institutes, South China Normal University, Guangzhou 510006, P. R. China

ABSTRACT: A new photochemistry-based method was introduced for fabricating SnO_2 monolayer ordered porous films with size-tunable surface pores on ceramic tubes used for gas sensors. The growth of the spherical pore walls was controlled by two times irradiation of the ultraviolet light using polystyrene microsphere two-dimensional colloidal crystal as a template. The surface pore size of the final obtained porous films was well tuned by changing the second irradiation time rather than replacing the template microspheres. The monolayer ordered porous films on the tubes were directly used, for the first time, as gas sensors. The sensitivity of the sensor depended on the surface pore size and was carefully analyzed by ethanol gas detection. The sensor also exhibited short response−recovery time and long-term stability at lower than 300 °C in practical applications. Therefore, this study opens up a kind of construction method for gas sensors, provides a new strategy for controlling the surface pore size of the monolayer ordered porous film, and introduces a new type of sensitivity-controllable gas sensor.

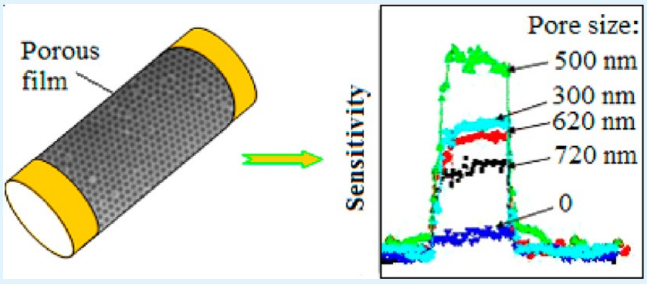

KEYWORDS: *colloidal crystal, monolayer ordered porous film, SnO_2, photochemical preparation, air−water interface, gas sensor*

INTRODUCTION

Porous films with pore sizes in the micrometer and submicrometer ranges have recently elicited much interest because of their use as membranes for separation and purification,[1,2] solid for sensors,[3−5] scaffolds for tissue engineering,[6,7] photonic band gap materials,[8−10] and so on. The fabrication of these porous films typically involves conventional methods based on emulsion solution foaming,[11] ceramic particle sintering,[12] and etching.[13] In the past 15 years, latex microsphere colloidal crystal template methods have exhibited many advantages in the fabrication of 2D or 3D highly ordered porous structure materials and have gained a great deal of attention from researchers.[14−17] Colloidal monolayer can be transferred from one substrate to another, or to a solution surface,[18] showing excellent flexibility when used as template. Therefore, several monolayer ordered porous films have been fabricated on various substrates,[19−22] including the curved[23,24] and solution surfaces.[25,26] However, the surface pore size of films have limited manipulation features and can only be controlled by the template microspheres, which would obviously change the characteristic periodic parameter of the porous film and add to the unpredictability in controlling the corresponding property of the film, aside from the complexity in manipulations. Although the electrodeposition method[27,28] can control the pore sizes, the film is only fabricated on the conductor substrate, thereby restricting its wide applications. Therefore, the fabrication of monolayer ordered porous film with tunable surface pore size on various substrates without changing the template microspheres, as well as the exploration of its application, is necessary and remains a challenge.

Resistive-type gas sensor represents a category of devices for the detection of environmental gases. Ceramic tube with curved surface is a conventional and widely used substrate for loading the sensing materials. However, the sensing materials are usually processed into pastes and then coated on the surface of the ceramic tube,[29−31] resulting in the formation of film with inhomogeneous structural unities and the difficulty in controlling the sensitivity. Multilayer ordered porous films based on colloidal crystal templates have been fabricated on the ceramic tube[23,32] by thermal chemical method, providing relatively homogeneous sensing surfaces. However, the layer-by-layer preparation procedures are time-consuming and

Received: November 12, 2013
Accepted: December 27, 2013
Published: January 10, 2014

   dx.doi.org/10.1021/am4050844 | ACS Appl. Mater. Interfaces 2014, 6, 1251−1257

arduous, and the response and recovery times are relatively long, which severely limit their practical applications. When a monolayer porous film is applied on the tube, the tube inevitably exhibits too many cracks, is not conductive, and is unsuitable for application in gas sensing due to the limitations of the thermal−chemical fabrication techniques. Moreover, the application and the relevant performances of the monolayer porous film on the gas-sensing ceramic tube have been not reported yet.

SnO_2 is a conventional gas-sensing semiconductor material, and various new micro-/nanostructured SnO_2 prepared by new methods are constantly emerging to enhance its performances.[33−36] In the present work, a novel photochemistry-based method has been introduced for producing SnO_2 monolayer ordered porous film with size-tunable surface pores on the curved surface of a ceramic tube used for gas sensing. When the polystyrene (PS) microsphere colloidal monolayer was used as a template, the SnO_2 shells grew around the microspheres and stopped at a specific position of the template spheres under the irradiation of UV light. The final surface pore size (i.e., the diameter of the pore openings in the surface of the film) of the monolayer ordered porous films was thus controlled without changing the sizes of the template microspheres. Given that the film was stabilized on the tube through direct growth at room temperature, fewer cracks have been generated compared with that obtained from the thermal−chemical method. Such monolayer ordered porous films on tubes can be directly used as gas sensors, exhibiting various sensitivities with the surface pore size, second-level response rate, and excellent stability. Compared with the conventional method for preparing ordered porous structure, the proposed method is low-cost, environment-friendly, efficient, simple, and practical.

EXPERIMENTAL SECTION

Fabrication of Monolayer Colloidal Crystal. Ordinary glass substrates were ultrasonically cleaned in acetone and then in ethanol for 1 h. Monodispersed PS-microsphere (750 nm in diameter) suspensions (2.5 wt % in water, surfactant free) were bought from Alfa Aesar Company. The glass substrate was cut into 1.5 × 1.5 cm^2 pieces, and then a piece of substrate was mounted on a custom-built spin coater. An amount of 10 μL of PS-microsphere suspensions was dropped onto the substrate. Large area monolayer (more than 1 cm^2) colloidal crystal could be fabricated by a spin-coating method at a speed of 800 rotations per minute.

Fabrication of SnO_2 Monolayer Ordered Porous Film on Ceramic Tube. The commercially supplied ceramic tube with outer diameter of 2 mm and length of 5 mm (Scheme 1a) was directly employed as the substrate. The precursor solution was typically prepared with 0.22 g of $SnSO_4$ dissolved in 20 mL of 0.37 M H_2SO_4 aqueous solution. The fabrication process of the porous film is shown in Scheme 1b−f. The monolayer colloidal crystal was first floated onto the surface of the precursor solution, lasting about 45 min as reported elsewhere.[26] Subsequently, the template was irradiated with two UV lamps (8 W, 254 nm) for 0.5 h (defined as the FIRST irradiation). And then the composite film (composed of the colloidal monolayer and SnO_2 fundamental shells) was picked up with the ceramic tube to undergo the SECOND irradiation under the same UV lamps. The composite film should cover and connect the gold films on the two ends of the tube in order to ensure that the resulting film is conductive. Finally, the ceramic tube was dried at 120 °C for 1 h and then heated at 300 °C for 1 h in a furnace to remove the template. Different porous films with controlled pore-opening diameter (d) and height (h) were obtained by controlling the second irradiation time at 0.5, 1.5, 8.5, 15.5, and 23.5 h, respectively.

Gas-Sensing Test. A platinum (Pt) heater wire was crossed through the ceramic tube covered with the porous film. Subsequently, the Pt wire and electrode wires were all welded onto a support used for a gas-sensing test system. A gas sensor was thus constructed. The gas sensing test was operated on a WS-30A system (Weisheng Instruments Co., Zhengzhou, China). A stationary state gas distribution method was carried out for gas response testing. The ethanol gas to be detected was injected into a test chamber and mixed with air. The working temperature of the sensors was adjusted by varying the heating voltage at the Pt wire and monitored with a thermometer. The performance of the gas-sensors was studied by changing the sensors with different surface pore sizes, ethanol gas concentrations, and working temperatures.

Scheme 1[a]

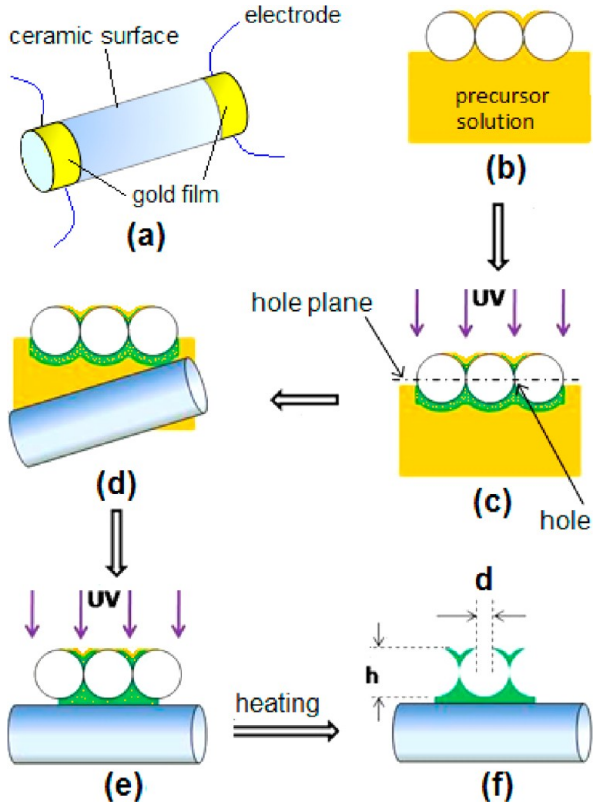

[a]Schematic of the ceramic tube used as the substrate (a) and the fabrication process of the monolayer SnO_2 ordered porous film. (b) The colloidal monolayer floated on the solution. (c) The SnO_2 fundamental shells formed around the microspheres under the FIRST irradiation. (d) The SnO_2 shell/colloidal monolayer was picked up. (e) The SnO_2 shells further grew under the SECOND irradiation. (f) Final porous structure on the tube.

Characterizations. The morphologies of the resulting porous films on the ceramic tubes were examined by scanning electron microscopy (SEM, Shimadzu SS-550 and Quanta 250 FEG). The compositions were characterized by X-ray powder diffraction (XRD, D/max2200, with Cu Kα radiation). Samples for the XRD measurements were prepared on the glass substrates under the same conditions as those for preparation on the ceramic tubes.

RESULTS AND DISCUSSION

Figure 1a shows the SEM image of a specific ceramic tube covered with a final monolayer ordered porous film. The film covered the entire surface of the tube and connected the gold films on the two ends. The electrode wires welded on the gold films could be discerned. Parts b−f of Figure 1 show the SEM images of the porous films on the tubes obtained with different SECOND irradiation times. All films were fabricated from the 750 nm PS-microsphere colloidal crystal templates and

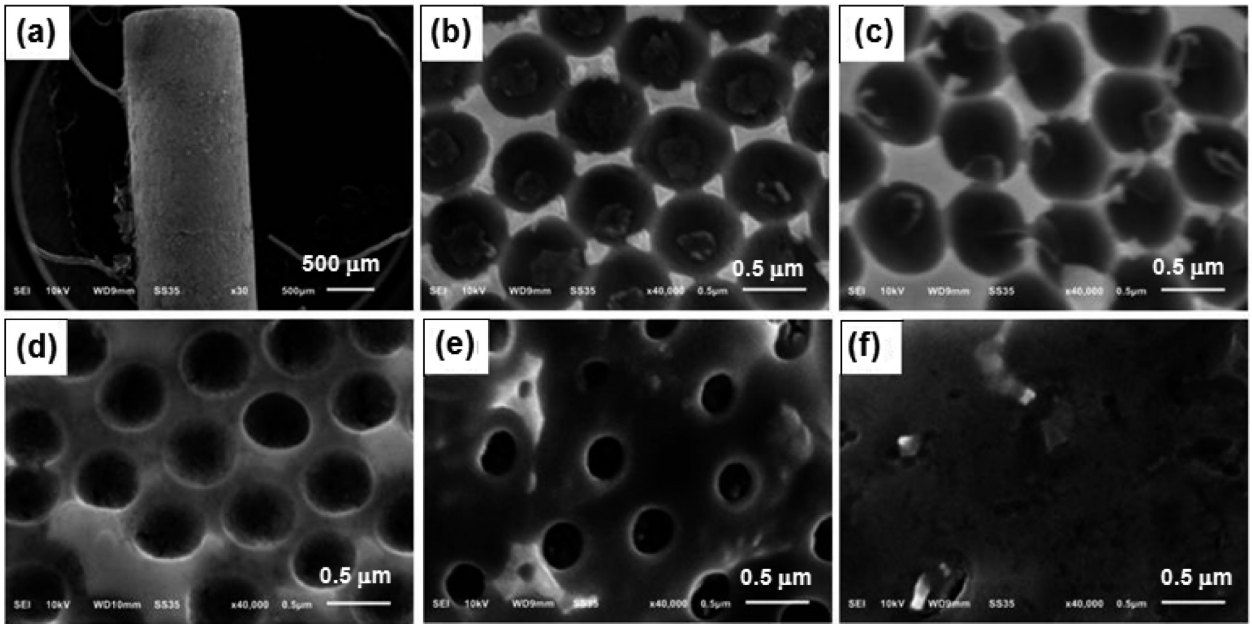

Figure 1. SEM images of the monolayer SnO_2 ordered porous films on ceramic tubes with different SECOND irradiation times: (a) low-magnification image of the ceramic tube covered with the porous film with the SECOND irradiation time of 0.5 h; (b–f) images of the porous films obtained from the SECOND irradiations of 0.5, 1.5, 8.5, 15.5, and 23.5 h, respectively.

experienced the same FIRST irradiation (0.5 h) and the same thermal treatments. The visible spherical pores were arranged hexagonally in one film, and the center-to-center spacing between two adjacent pores was kept at 750 nm. They had the same sizes in a sample but regularly varied with the SECOND irradiation time in different samples. When the time increased from 0.5 to 23.5 h, the surface pore size gradually decreased from ~720 to ~620, ~500, ~300, and 0 nm; by calculation, the height of the pores increased from ~270 to ~586, ~655, ~719, and 750 nm. The pore openings of the adjacent pores were gradually far away from each other until no pore was found in the film. In addition, there were some particles among three adjacent pores and on the wedges formed with two adjacent pores for samples obtained with shorter SECOND irradiation time ($\leq$1.5 h) (parts b and c of Figure 1); other samples had flat surfaces among all pores.

The growth process of monolayer SnO_2 porous films is illustrated as follows. When UV light was utilized to irradiate the template-floated solution, a series of photochemical and chemical reactions occurred (eqs 1–3).[37] Sn^{2+} in the precursor solution adsorbs photons to produce Sn^{4+} and solvated electrons. The electrons are then captured by Sn^{2+} to form metallic tin nuclei. The freshly formed metallic tin possesses high activity and can immediately react with O_2 in the air to be transformed into SnO_2 at the air–water interface.

$$Sn^{2+} + h\nu \rightarrow Sn^{4+} + 2e \quad (1)$$

$$Sn^{2+} + 2e \rightarrow Sn^{0} \quad (2)$$

$$Sn^{0} + O_2 \rightarrow SnO_2 \quad (3)$$

SnO_2 fundamental shells formed around the template microspheres. Because the PS microspheres were closely packed in the template, SnO_2 cannot form on the place where two adjacent microspheres are contacted, thereby resulting in six evenly distributed holes on a single shell.[38] Taking an imaginary plane consisting of the holes (hole plane) as boundary (Scheme 1c), the shells can be divided into two parts, namely, the upper layer with circle open and the lower layer with spherical bottom. Subsequently, when the composite film formed in the process of the FIRST irradiation was picked up, the interstitial space in the film was still completely filled with the precursor solution because of capillary effects. Under the SECOND irradiation, new SnO_2 crystal nuclei preferably formed and grew on the pre-existent shells. With the assistance of capillary action, the solution can always reach the leading edges of the shells. Thus, the height (h) and the thickness of the shells were increased continually. Simultaneously, the defects of the pre-existent shells can be improved by the secondary growth. SnO_2 also directly grew on the surface of the ceramic tube, in which the composite film was stabilized on the tube. During the drying at 120 °C and the removal of PS microspheres at 300 °C, the residual tin ions would be hydrolyzed into stannic acid and transformed into SnO_2.[37] The defects in the shells were further improved.

Obviously, the SECOND irradiation time was responsible for the control of the surface pore size. When the SECOND irradiation was short, for example, 0.5 h, the shells (the final pore walls) were very thin and the connections between the upper layer and the lower layer were very weak; thus, the upper layer on the hole plane can be easily removed with the removal of the template. As a result, only the lower layer of the porous film can be kept in the tube, and the surface pore size was measured as ~720 nm (Figure 1b). The particles among the three adjacent pores were the residuals of the upper layer. The pore size was smaller than the diameter of the PS, indicating that the height of the pore was lower than that of a semi-microsphere. When the irradiation time was increased to 1.5 h, the pores in the lower layer grew higher than the semimicrosphere, but their walls were still too thin to be kept integrally. The surface pores showed a diameter of ~620 nm, and some residual upper layers remained (Figure 1c). The shells had enough thickness when the irradiation time was continuously increased to 9 h; thus, the upper layer cannot be removed.

Meanwhile, the height increased, which was clearly higher than the semimicrosphere. Decided by the character of a sphere, the final surface pore size decreased to ~500 nm (Figure 1d). For the same reason, the surface pore size decreased to ~300 nm when the irradiation time was controlled at 15.5 h (Figure 1e). After 23.5 h, no surface pores, but only a dense film, were found (Figure 1f). Whether the porous structures experienced the SECOND irradiation or not, they showed similar X-ray diffraction (XRD) pattern (Figure 2) corresponding to the tetragonal cassiterite structure of SnO_2 (JCPDS no. 72-1147).

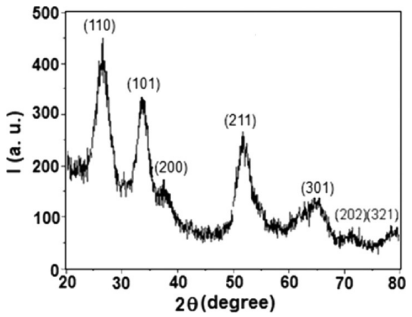

Figure 2. XRD spectrum of the porous film fabricated on a glass substrate similar to that fabricated on the ceramic tube. All films had the similar XRD spectra.

Notably, the final porous films would be directly used for gas detection; thus, every step of the fabrication process is important and necessary. The FIRST irradiation was used to induce the formation of a porous skeleton with spherical bottom. However, with this step ignored, the PS microspheres would directly contact the surface of the tube in the following manipulation, resulting in the formation of a through-pore film. The through-pores directly expose the local surfaces of the tube in the surrounding gas,[28] thereby reducing the contact area between the SnO_2 film and the gas, which is disadvantageous for in gas-detecting application. However, if only the FIRST irradiation is used and the SECOND irradiation is omitted, obtaining a perfect film suitably used in gas sensor would still be difficult. Figure 3a shows the SEM image of the monolayer porous film on the ceramic tube obtained according to Scheme 1 but omitting the SECOND irradiation. Spherical pores can be easily discerned. The shells were deformed and the upper layer was removed during the removal of the PS microspheres because the shells were very thin. In addition, the edge of the film was slightly peeled off (Figure 3b), indicating that the film could not be firmly stabilized on the tube. However, the thickness of the shells was increased after the SECOND irradiation. Figure 3c shows the side view of the porous film after the SECOND irradiation of 8.5 h. The spherical shape of the pores can be held well, and the whole film was firmly stabilized on the surface of the ceramic tube.

The ceramic tube covered with the monolayer ordered porous film can be directly constructed into a kind of resistive-type gas sensor used for the detection of ethanol gas in the surroundings (Figure 4a). The sensor responses to different concentrations (100, 200, and 400 ppm) of ethanol gas at 260 °C are shown in Figure 4b. The sensors were constructed with monolayer porous films with surface pores of 720, 620, 500, 300, and 0 nm, respectively. The gas sensitivity[39] is defined as $S = R_{air}/R_{gas}$, where R_{air} and R_{gas} are the resistances of the sensor in the air and the air mixed with ethanol gas, respectively. The response time is defined as the time required for reaching 90% of the equilibrium value;[40] the recovery time is defined as the time taken for the sensor output to be decreased to 10% of its steady value.[41] All sensors can quickly respond to the introduced ethanol gas, and the response time is always limited within 10 s in detecting different concentrations of gas. They could also quickly recover within 10 s after the gas was removed. The sensitivity regularly varied with the surface pore size of the film (i.e., the SECOND irradiation time) in detecting a specific gas concentration. When the surface pore size decreased from 720 to 500 nm (i.e., the SECOND irradiation time increased from 0.5 to 8.5 h), the sensitivity gradually increased to the maximum value. Afterward, the sensitivity decreased with the decrease of the surface pore size. However, without surface pore, the sensor exhibited the lowest sensitivity. This regularity implies that sensitivity of such nanostructured sensors can be easily controlled by changing the size of the surface pores. Additionally, the response time was also related to the surface pore size. Taking the detection of 400 ppm gas as an example, as the surface pore size decreased from 720 to 300 nm, the response time increased from 6.7 to 8.6 s. The film without surface pores had the shortest response time, 3.0 s.

For a specific sensor, the sensitivity noticeably increased with the increase of the gas concentration. Taking the sensor with 500 nm surface pores as an example, the sensitivity increased from ~5.2 to ~7.0 and ~8.6 when the concentration was increased from 100 ppm to 200 ppm and 400 ppm (Figure 4c). Compared with other sensors, the sensor had the maximum varied values in detecting different concentrations of gas, indicating that this condition was more favorable with the quantitative gas detection.

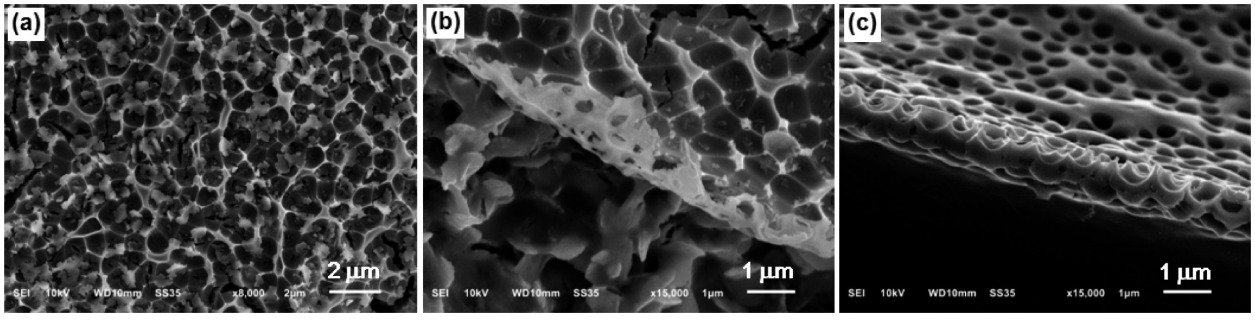

Figure 3. (a) Film obtained without the SECOND irradiation in the fabrication process. (b) Edge of the film in (a). (c) Side view of an edge of the film obtained with the SECOND irradiation time of 8.5 h.

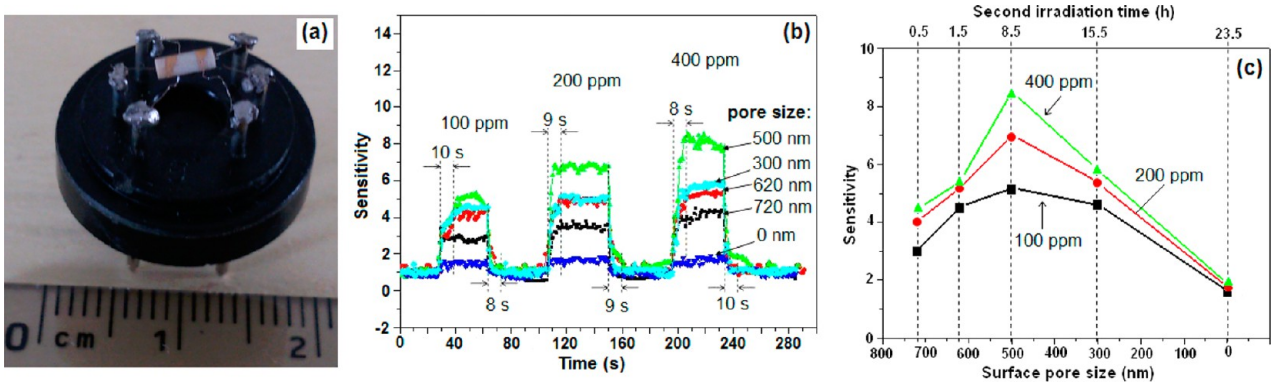

Figure 4. Photo of a gas sensor (a) and the gas-sensing performances of the SnO_2 monolayer porous films in detecting ethanol gas. (b) Responses of the films with different surface pore sizes to different concentrations of ethanol gas. (c) Variations of the sensitivities with the surface pore size or the SECOND irradiation time.

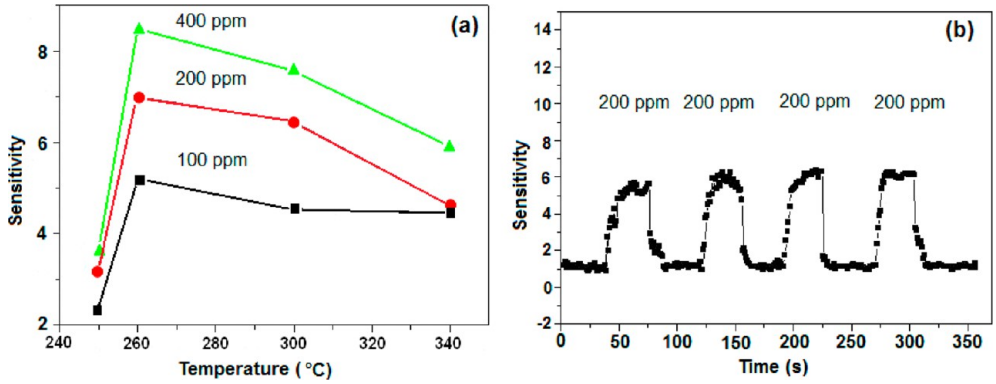

Figure 5. (a) Effects of working temperature on the sensitivity and (b) reuse of the gas sensor obtained with an irradiation time of 8.5 h.

Scheme 2. Schematic of the Adsorptions for Oxygen Species by a Single Pore Obtained with Different SECOND Irradiation Times

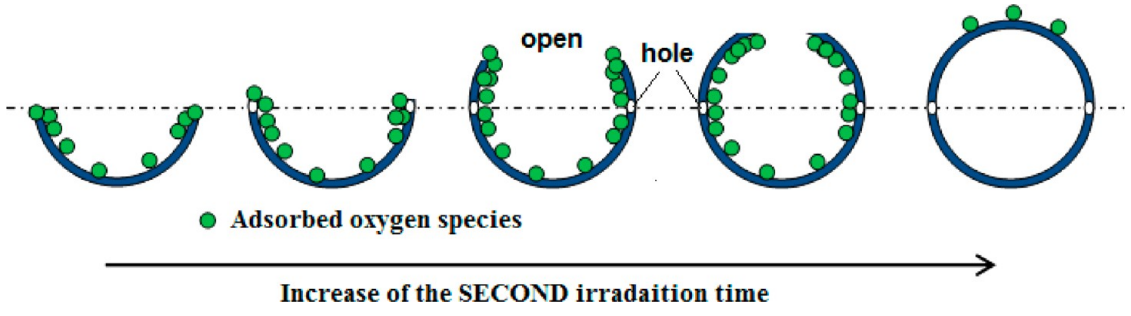

For further practical application, responses of the porous SnO_2 film to the different concentrations of ethanol gas at different working temperatures should be studied. In this study, the sensor with 500 nm surface pores was chosen and the working temperatures were controlled in the range of 250−340 °C by changing the working voltage of the heater wire. In detection of any specific concentration of gas, the sensitivity of the sensor increased first when the temperature increased from 250 to 260 °C and then decreased with the increase in temperature, as shown in Figure 5a. The maximum sensitivity values of 5.2, 7.0, and 8.5 were obtained at 260 °C in detecting 100, 200, and 400 ppm of ethanol gas, respectively. The sensors exhibited excellent stability (Figure 5b). After the sensor experienced all the tests shown in Figure 4b, Figure 4c, and Figure 5a (at least 18 times of reuse) and placed in ordinary surroundings for more than 40 days without any protection, the sensor still exhibited nearly the same sensitivity as that when it was first used before 40 days in detecting 200 nm of ethanol gas. Thus, the sensor may be reused continuously.

The sensing mechanism and the controllability in sensitivity of the sensor were suggested as follows. When the n-type SnO_2 semiconductor is used in gas sensor and exposed in air, O_2 molecules will be chemisorbed and capture some electrons of SnO_2 to be changed into O_2^-, O^-, and O^{2-} on the sensing body surfaces.[42] The oxygen species can then establish a chemical equilibrium:

$$O_2 \overset{e}{\leftrightarrow} O_2^- \overset{e}{\leftrightarrow} O^- \overset{e}{\leftrightarrow} O^{2-} \quad (4)$$

After the reducing gas (e.g., ethanol gas) is introduced, some oxygen species will be reduced and removed from the surfaces above a certain temperature, resulting in the variation of the

dx.doi.org/10.1021/am4050844 | ACS Appl. Mater. Interfaces 2014, 6, 1251−1257

resistance of SnO_2. The surface area and the morphology of a sensing film can directly decide the adsorption quantity of the oxygen species and hence have important impacts on the variation of resistance and the relevant sensitivity of the sensors.

For the sensors in this study, the adsorption of the monolayer porous film for the oxygen species can be illustrated as Scheme 2. The oxygen species can always be adsorbed on the exposed surface, including the pore walls, pore edges, and pore defects. The edges and defects had higher surface energy and can adsorb more O_2 molecules. For all films, the numbers of pores per unit area were equal. The surface area of the porous film would be decided principally by the height of the spherical pores. The higher the pores are, the higher the surface area is and the higher the numbers of adsorbed oxygen species on pore walls are. During the increase of the height of the pores, the opening of the pores became smaller and the length of the pore edges became shorter, thereby reducing the adsorption numbers. Pore defects mainly came from the generation of holes on the pore walls. Their sizes and adsorption abilities cannot be changed with the increase in the pore height if the upper layers of films were integrally preserved. The total adsorption numbers would decide the sensitivity of the sensors. With the increase in the SECOND irradiation time from 0.5 to 8.5 h, the surface area of the obtained porous film also increased and the holes on pore walls gradually formed. Although the length of the pore edges had been decreasing, the increase in the numbers of oxygen species adsorbed on the pore walls and pore defects could prevail, resulting in the increase in the sensitivity of the sensors. When the irradiation time was increased to 15.5 h, the pore opening decreased to ~300 nm. Compared with the film with 500 nm surface pores, the decrease of adsorption numbers on pore edges in this film may suppress the increase in those on pore walls. Meanwhile, the decreased pore openings and the increased pore depth would make it difficult for the introduced ethanol gas to go through the opening and reach the pore bottom when the sensor worked. As a result, the sensitivity of the sensor decreases. When the film had no surface pore, only the flat surface with smaller area was exposed in the surroundings, resulting in very low sensitivity of the film. In addition, the fine structures of pore walls might also give impacts on the sensitivity. Pore walls were actually composed of fine particles and micro-/mesopores formed by the piling of these particles. With the increase of the film thickness, the amount of the micro-/mesopores was naturally increased, which could increase the total surface area of the film and bring positive impacts on the sensitivity. However, size of the micro-/mesopores was so small that the gas molecules could not easily go through these pores. Therefore, the effect of the fine structures on the sensitivity of the film was very faint and morphologies of the macropores should be still decisive. The morphology of the surface pore also affected the response time. For the film without surface pores, the ethanol gas could quickly pass through the flat surface and react with the adsorbed oxygen species, so it has the shortest response time. For the porous film, as the surface pore size decreased, surface area and the time that the ethanol gas covered the surface increased, resulting in the gradual increase of the response time.

CONCLUSIONS

In summary, using a photochemistry-based method and the PS-microsphere (with diameter of 750 nm) colloidal monolayer as template, SnO_2 monolayer ordered porous films with different sizes of surface pores were fabricated on the ceramic tubes by two times UV irradiation. With the increase in the SECOND irradiation time, the pore walls were heightened gradually and the size of the surface pores were tuned in the range of 720−0 nm, without changing the size of the template microspheres. These films on the ceramic tube were used as gas sensor to detect the ethanol gas. The films exhibited excellent performance, such as tunable sensitivity by controlling the size of the surface pores (or the SECOND irradiation time), quick response and recovery time within 10 s, and continuous stability in the course of reuse, which would contribute to their practical applications. Our preliminary studies showed that other oxides and sulfides, such as Fe_2O_3, Cu_2O, CdS, CuS, and ZnS, can also be constructed into monolayer ordered porous film gas sensors for the detection of different environment gases.

AUTHOR INFORMATION

Corresponding Author

*E-mail: fqsun@scnu.edu.cn. Phone: 86-20-39310187. Fax: 86-20-39310187.

Author Contributions

The manuscript was written through contributions of all authors.

Notes

The authors declare no competing financial interest.

ACKNOWLEDGMENTS

This work was cosupported by the National Natural Science Foundation of China (Grant 31071057), the Research Project of Chinese Ministry of Education (Grant 213029A), and the Natural Science Foundation of Guangdong Province (Grants 10351063101000001 and S2011010003499).

REFERENCES

(1) Wan, L. S.; Li, J. W.; Ke, B. B.; Xu, Z. K. *J. Am. Chem. Soc.* **2012**, *134*, 95−98.
(2) Gaborski, T. R.; Snyder, J. L.; Striemer, C. C.; Fang, D. Z.; Hoffman, M.; Fauchet, P. M.; Mcgrath, J. L. *ACS Nano* **2010**, *4*, 6973−6981.
(3) Xing, R. Q.; Xu, L.; Zhu, Y. S.; Song, J.; Qin, W. F.; Dai, Q. L.; Liu, D. L.; Song, H. W. *Sens. Actuators, B* **2013**, *188*, 235−241.
(4) Iizuka, K.; Kambara, M.; Yoshida, T. *Sens. Actuators, B* **2013**, *182*, 250−255.
(5) Paul, R. K.; Badhulika, S. N.; Saucedo, M.; Mulchandani, A. *Anal. Chem.* **2012**, *84*, 8171−8178.
(6) Choi, S. W.; Zhang, Y.; Xia, Y. N. *Langmuir* **2010**, *26*, 19001−19006.
(7) Speranza, V.; Trotta, F.; Drioli, E.; Gugliuzza, A. *ACS Appl. Mater. Interfaces* **2010**, *2*, 459−466.
(8) Deutsch, M.; Vlasov, Y. A.; Norris, D. J. *Adv. Mater.* **2000**, *12*, 1176−1180.
(9) van den Broek, J. M.; Woldering, L. A.; Tjerkstra, R. W.; Segerink, F. B.; Setija, I. D.; Vos, W. L. *Adv. Funct. Mater.* **2012**, *22*, 25−31.
(10) Zheng, L. X.; Cheng, H.; Liang, F. X.; Shu, S. W.; Tsang, C. K.; Li, H.; Lee, S. T.; Li, Y. Y. *J. Phys. Chem. C* **2012**, *116*, 5509−5515.
(11) Imhof, A.; Pine, D. J. *Nature* **1997**, *389*, 948−951.
(12) Garino, T. J.; Bowen, H. K. *J. Am. Ceram. Soc.* **1987**, *70*, C-315−C-317.
(13) Yoshida, M.; Asano, M.; Suwa, T.; Reber, N.; Spohr, R.; Katakai, R. *Adv. Mater.* **1997**, *9*, 757−758.
(14) Davis, M. E. *Nature* **2002**, *417*, 813−821.
(15) Ren, Z. Y.; Li, X.; Zhang, J. H.; Li, W.; Zhang, X. M.; Yang, B. *Langmuir* **2007**, *23*, 8272−8276.

(16) Zhang, J. H.; Li, Y. F.; Zhang, X. M.; Yang, B. *Adv. Mater.* **2010**, *22*, 4249−4269.
(17) Zhang, Y. S.; Regan, K. P.; Xia, Y. N. *Macromol. Rapid Commun.* **2013**, *34*, 485−491.
(18) Burmeister, F.; Schäfle, C.; Matthes, T.; Böhmisch, M.; Boneberg, J.; Leiderer, P. *Langmuir* **1997**, *13*, 2983−2987.
(19) Ye, X. Z.; Qi, L. M. *Nano Today* **2011**, *6*, 608−631.
(20) Li, Y.; Cai, W. P.; Duan, G. T. *Chem. Mater.* **2008**, *20*, 615−624.
(21) Ye, X. Z.; Li, Y.; Dong, J. Y.; Xiao, J. Y.; Ma, Y. R.; Qi, L. M. *J. Mater. Chem. C* **2013**, *1*, 6112−6119.
(22) Li, Y.; Koshizaki, N.; Wang, H. Q.; Shimizu, Y. *ACS Nano* **2011**, *5*, 9403−9412.
(23) Sun, F.; Cai, W.; Li, Y.; Jia, L.; Lu, F. *Adv. Mater.* **2005**, *17*, 2872−2877.
(24) Bhawalkar, S. P.; Qian, J.; Heiber, M. C.; Jia, L. *Langmuir* **2010**, *26*, 16662−16666.
(25) Sun, F. Q.; Yu, J. C. *Angew. Chem., Int. Ed.* **2007**, *46*, 773−777.
(26) Li, C.; Hong, G. S.; Qi, L. M. *Chem. Mater.* **2010**, *22*, 476−481.
(27) Duan, G. T.; Cai, W. P.; Luo, Y. Y.; Sun, F. Q. *Adv. Funct. Mater.* **2007**, *17*, 644−650.
(28) Sun, F. Q.; Cai, W. P.; Li, Y.; Cao, B. Q.; Lu, F.; Duan, G. T.; Zhang, L. D. *Adv. Mater.* **2004**, *16*, 1116−1121.
(29) Yang, Z. X.; Huang, Y.; Chen, G. N.; Guo, Z. P.; Cheng, S. Y.; Huang, S. Z. *Sens. Actuators, B* **2009**, *140*, 549−556.
(30) Wang, L. L.; Lou, Z.; Fei, T.; Zhang, T. *J. Mater. Chem* **2011**, *21*, 19331−19336.
(31) Wang, X. F.; Xie, Z.; Huang, H. T.; Liu, Z.; Chen, D.; Shen, G. Z. *J. Mater. Chem.* **2012**, *22*, 6845−6850.
(32) Jia, L. C.; Cai, W. P. *Adv. Funct. Mater.* **2010**, *20*, 3765−3773.
(33) Xu, J.; Li, Y. S.; Huang, H. T.; Zhu, Y. G.; Wang, Z. R.; Xie, Z.; Wang, X. F.; Chen, D.; Shen, G. Z. *J. Mater. Chem.* **2011**, *21*, 19086−19092.
(34) Chen, D.; Xu, J.; Xie, Z.; Shen, G. Z. *ACS Appl. Mater. Interfaces* **2011**, *3*, 2112−2117.
(35) Wang, Z. J.; Li, Z. Y.; Jiang, T. T.; Xu, X. R.; Wang, C. *ACS Appl. Mater. Interfaces* **2013**, *5*, 2013−2021.
(36) Manjula, P.; Boppella, R.; Manorama, S. V. *ACS Appl. Mater. Interfaces* **2012**, *4*, 6252−6260.
(37) Wang, H. J.; Sun, F. Q.; Zhang, Y.; Li, L. S.; Chen, H. Y.; Wu, Q. S.; Yu, J. C. *J. Mater. Chem.* **2010**, *20*, 5641−5645.
(38) Sun, F.; Cai, W.; Li, Y.; Cao, B.; Lei, Y.; Zhang, L. *Adv. Funct. Mater.* **2004**, *14*, 283−288.
(39) Lai, X. Y.; Li, J.; Korgel, B. A.; Dong, Z. H.; Li, Z. M.; Su, F. B.; Du, J.; Wang, D. *Angew. Chem., Int. Ed.* **2011**, *123*, 2790−2793.
(40) Wu, W. Y.; Ting, J. M.; Huang, P. J. *Nanoscale Res. Lett.* **2009**, *4*, 513−517.
(41) Zhang, Y.; Li, J. P.; An, G. M.; He, X. L. *Sens. Actuators, B* **2010**, *144*, 43−48.
(42) Huang, X. J.; Meng, F. L.; Pi, Z. X.; Xu, W. H.; Liu, J. H. *Sens. Actuators, B* **2004**, *99*, 444−450.